IEEE Robotics and Automation Letters (RA-L) paper, presented at ICRA 2026, Vienna, Austria. Cite as RA-L paper.

A Framework for Adaptive Load Redistribution in Human-Exoskeleton-Cobot Systems

Emir Mobedi, Gokhan Solak, *Member, IEEE*, and Arash Ajoudani, *Member, IEEE*

***Abstract*—Wearable devices like exoskeletons are designed to reduce excessive loads on specific joints of the body. Specifically, single- or two-degrees-of-freedom (DOF) upper-body industrial exoskeletons typically focus on compensating for the strain on the elbow and shoulder joints. However, during daily activities, there is no assurance that external loads are correctly aligned with the supported joints. Optimizing work processes to ensure that external loads are primarily (to the extent that they can be compensated by the exoskeleton) directed onto the supported joints can significantly enhance the overall usability of these devices and the ergonomics of their users. Collaborative robots (cobots) can play a role in this optimization, complementing the collaborative aspects of human work. In this study, we propose an adaptive and coordinated control system for the human-cobot-exoskeleton interaction. This system adjusts the task coordinates to maximize the utilization of the supported joints. When the torque limits of the exoskeleton are exceeded, the framework continuously adapts the task frame, redistributing excessive loads to non-supported body joints to prevent overloading the supported ones. We validated our approach in an equivalent industrial painting task involving a single-DOF elbow exoskeleton, a cobot, and four subjects, each tested in four different initial arm configurations with five distinct optimisation weight matrices and two different payloads.**

***Index Terms*—Ergonomic human-robot collaboration, human factors and human-in-the-loop, physically assistive devices, wearable robotics.**

I. Introduction

MANUAL operations such as packaging [1], assembly [2] and painting [3] are essential in many industries, though they can place a significant strain on the physical health of human workers. Research highlights the financial strain of these issues, for instance, a study found that recovery costs for painting workers suffering from repetitive muscle strain injuries range from 20,000 to 100,000 USD [3], [4]. Consequently, repetitive tasks are a major contributor to work-related musculoskeletal disorders (WMSDs), which affect approximately 20% of the global population [5], [6].

From a positive perspective, the introduction of collaborative robots (cobots) [7] and wearable assistive devices [8] over the past decade has enhanced safety and productivity in operations such as drilling [9], assembly [10], manual handling [11], helping therapists [12], and pick-and-place tasks [13], by reducing the risk of injuries and fatigue for human co-workers [14]. For example, in [15], a bi-manual human-robot cooperation task was developed for carrying a heavy box (10 kg). Optimization was applied to minimize the sum of hand contact forces with the box via the robot, and user ergonomics were evaluated using the Rapid Entire Body Assessment (REBA) method. Despite the low REBA scores indicating good ergonomics, the worker still needed to exert high torque due to the weight of the box. In [16], a control method was designed to reduce human fatigue when manipulating heavy objects in industrial tasks. Although this method improved user posture, repetitive tasks may still lead to WMSDs, as no additional physical support was provided to alleviate the remaining torque load. Similarly, in [17], a human-robot collaboration (HRC) control framework was developed for heavy material handling. The optimization minimized targeted joint torques, considering constraints such as human joint limits and robot workspace. The robot guided the human worker to an optimized body configuration; however, the method was limited to static conditions, and reliance on a force plate for joint torque estimation restricted the control framework's flexibility. Over subsequent years, this algorithm has been adapted for more dexterous tasks like drilling or polishing, incorporating additional constraints (e.g., human arm muscular manipulability and safety) to achieve an ergonomic working pose in the sagittal plane [18]. Despite significant torque reduction in both studies mentioned, high effort remains in specific joints (e.g., 15 Nm in the biceps in [18]). Finally, in [19], a control framework was developed to enable ergonomic and reconfigurable HRC. Although the online estimated torque values were optimized to guide the worker to ergonomic poses, the average optimized joint torques still posed a notable load, reported around 15 Nm in the shoulder and 12 Nm in the elbow. Alternatively, a box lifting task is carried out with an elbow exoskeleton, transferring support up to 12 Nm [11]. Yet, the torque of the shoulder joint is at high level. In [12], a soft assistive device is developed for shoulder joints to reduce the effort of the therapists in rehabilitation tasks. In this case, no assistance is provided for elbow joint.

Although the proposed solutions are promising, it is clear that neither cobots nor exoskeletons alone have achieved full minimization of the loads imposed on human body joints in

Received 15 November 2024; accepted 13 April 2025. Date of publication 24 April 2025; date of current version 2 May 2025. This article was recommended for publication by Associate Editor T. Verstraten and Editor J.-H. Ryu upon evaluation of the reviewers' comments. This work was supported by Horizon Europe Project Tornado under Grant 101189557. *(Corresponding author: Emir Mobedi.)*

This work involved human subjects or animals in its research. Approval of all ethical and experimental procedures and protocols was granted by the Human-Robot Interfaces and Interaction Lab (HRII), Istituto Italiano di Tecnologia (IIT), and approved by the ethics committee Azienda Sanitaria Locale (ASL) Genovese under Application No. 3, and performed in line with the Protocol IIT HRII SOPHIA 554/2020.

Emir Mobedi is with the Izmir Institute of Technology, Izmir 35430, Türkiye (e-mail: emirmobedi@iyte.edu.tr).

Gokhan Solak and Arash Ajoudani are with the Istituto Italiano di Tecnologia, 2003 Genoa, Italy (e-mail: gokhan.solak@iit.it).

This article has supplementary downloadable material available at https://doi.org/10.1109/LRA.2025.3564206, provided by the authors.

Digital Object Identifier 10.1109/LRA.2025.3564206

IEEE Robotics and Automation Letters (RA-L) paper, presented at ICRA 2026, Vienna, Austria. Cite as RA-L paper.

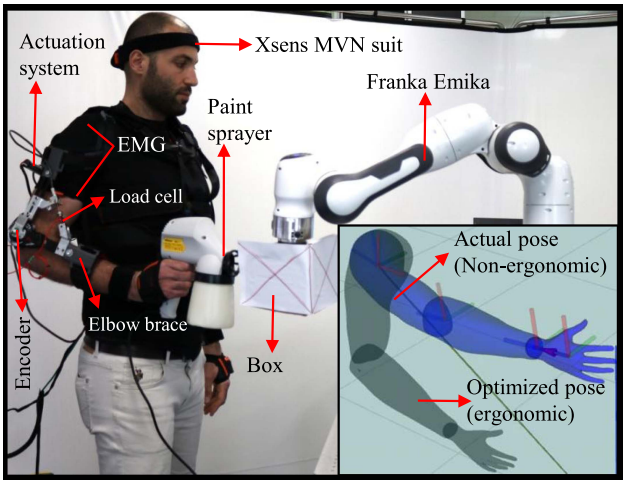

Fig. 1. This letter presents a solution that integrates exoskeletons for joint support, humans for supervisory roles, and cobots for adaptive task planning to optimize joint usage. It ensures that external loads are primarily directed onto the supported joints, to the extent that the exoskeleton can compensate. Through adaptive control, the cobot helps align the actual human pose (blue) with the optimized solution which is fed back to the user (grey).

collaborative tasks. Furthermore, when using exoskeletons with limited degrees of freedom (DOF), there is no assurance that external loads are properly aligned with the supported joints. For example, with an elbow exoskeleton, a task like painting may require movement in ways that place additional load on unsupported joints, such as the shoulder, which contradicts the purpose of using an exoskeleton.

This letter proposes a solution to address these challenges by integrating the strengths of exoskeletons (for localized joint support), humans (as supervisors), and cobots (for adaptive collaborative task planning). The approach focuses on supporting individuals equipped with wearable assistive devices on specific joints, while a cobot assists in optimizing task coordination to maximize the use of the supported joints (see Fig. 1). For example, if the wearable assistive device is positioned at the elbow, the cobot optimization does not need to prioritize torque minimization at that joint. Instead, it can focus more on other joints, such as the shoulder, as long as the maximum allowable torque in the supported joint remains within acceptable limits. To the best of our knowledge, this represents the first attempt to design a control framework that integrates both a robot and an exoskeleton operating together to minimize joint loading during 3D movements.

The control framework involves simplified human arm modelling, online optimization for overloading joints, ergonomic cobot planning, and the control of a 1-DOF elbow exoskeleton device [20]. The human right arm is modeled as a 6 DoFs rigid linkage bearing 3 DoFs in the shoulder, and 3 DoFs in the elbow. The human arm pose is then captured in real time using an Inertial Measurement Unit (IMU)-based system. Inverse kinematics is applied to estimate the joint angles needed for torque calculations. An online optimization technique, incorporating constraints like the robot's workspace and human joint limits, is used to distribute the interaction torques — referred to as overloading torques in this letter — arising from the weight of a handheld object between the shoulder and elbow joints. The optimized human joint angles are configurations where the overloading torques are primarily directed toward the supported elbow joint (due to the use of the elbow exoskeleton) until a threshold is reached, at which point the torques are redistributed also to the shoulder joints. Next, those joint angles are fed to the human model and displayed to the worker with the help of an avatar. Subsequently, the cobot moves the co-manipulated object in such a way to facilitate the alignment of the user's actual pose with that of the avatar (see Fig. 1 at the bottom right). In our work, the torque calculations are conducted under quasi-static assumptions, as manual tasks involving co-carrying or painting require slow movements due to the potential for heavy loads, as noted in [17].

As shown in Fig. 1, the actuation mechanism of the assistive device is attached to the back of the human worker, and its support force is transmitted to the elbow brace through the Bowden cable. The essential goal of the assistive mechanism is to alleviate the muscular effort of the human because of internal (i.e., 2 kg forearm weight in [21], [22]), and external (lightweight tools up to 1 kg) loading. This approach prevents prolonged exposure to repetitive loading, leading to fatigue, thereby enhancing the productivity of robotic co-workers in industrial settings. Additionally, force control is incorporated to leverage the human's supervisory capabilities. Specifically, the controller takes the elbow position as an input and outputs the assistive torque applied to the elbow joint. This enables the user to move his/her arm freely without encountering opposing forces, guiding it to an optimized pose with minimal physical or control-based constraints during the operation.

To show the applicability and the performance of the control technique, the verification is performed for a painting task on 4 subjects under 4 different arm configurations with different weight matrix defined in the optimization, and different payloads. Furthermore, the tests are conducted with and without exoskeleton assistance while measuring the effort through an electromyography interface in the shoulder and elbow.

The rest of the letter is structured as follows. In Section II, the methodology comprising human-arm modeling and its static force analysis, online optimization, robot planning, and exoskeleton control are studied. In Section III the experiments and the results are presented. Finally, in Section IV, the conclusions and future work are highlighted.

II. Methodology

The goal of this section is to introduce the details of the control framework including the static force analysis of the human right arm, online optimization for the minimization of the overloading joint torques, robot path planning, and the exoskeleton assistance.

A. Human Arm Model

The human right arm is modeled in URDF (Unified Robotics Description Format) as a 6 DoFs rigid link 3 DoFs of which are assigned for the shoulder (Σ_S), and the elbow (Σ_E) as in Fig. 2(a). Although we have 2 DoFs anatomically for the elbow including flexion/extension and supination/pronation, the XSENS human monitoring system [23] assigns 3 DoFs for each joint based on ISB biomechanical model [24]. Thus, it is mimicked in our URDF model.

To begin with, Σ_G is the global frame, and located exactly at the same point as Σ_S to compute the torques/forces of other frames with respect to Σ_G. On the other hand, Σ_W, and Σ_H

IEEE Robotics and Automation Letters (RA-L) paper, presented at ICRA 2026, Vienna, Austria. Cite as RA-L paper.

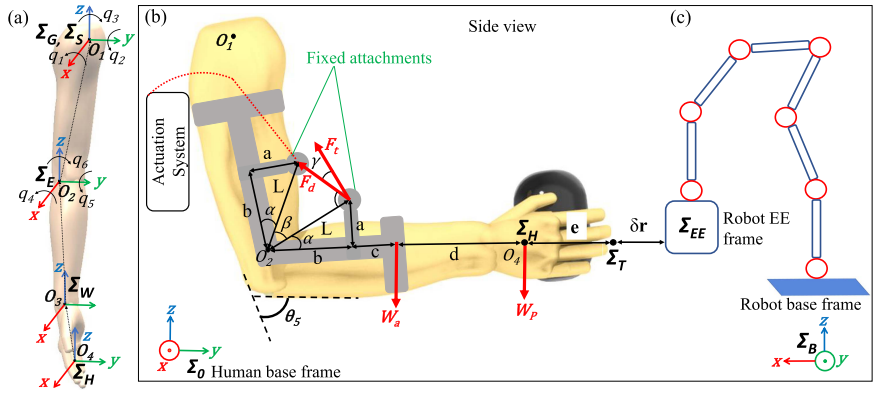

Fig. 2. (a) The isometric view of the right arm with the assigned coordinates. (b) The illustration of the arm attachments from side view. The dashed red line represents the Bowden cable that transfers the generated assistive force from the actuation system to the arm. The vertical distance between elbow brace (shown in gray color) and first anchor point on the forearm (a), the distance of fixed attachments from elbow frame Σ_E (b), the center of mass of the forearm (b+c), and the lever arm (b+c+d) from the external load (W_P) to O_2. (C) Shows the details of the robot with the assigned coordinates from side view. (e) Is the fixed distance between hand and target frame.

TABLE I
INPUTS OF THE OPTIMIZATION PROBLEM

HBPs [mm]	$l_{12_1}, l_{12_2}, l_{12_3}, l_{23_1}, l_{23_2}, l_{23_3}, l_{34_3}$: $24, 57, 301, 10, 4, 296, 90$			EPs [mm]	a, b, c, d : $50, 100, 50, 150$
ICs [m, rad]	$\boldsymbol{p}_L = [0.3 - 0.8 - 0.8]$, $\boldsymbol{p}_U = [0.9\ \ 0.8\ \ 0.8]$, $\boldsymbol{\theta}_L = [-0.22\pi - 0.5\pi - 0.06\pi\ \ 0 - 0.5\pi - 0.06\pi]$, $\boldsymbol{\theta}_U = [0\ \ 0.5\pi\ \ 0.06\pi\ \ 0\ \ 0\ \ 0]$				
	A	**B**	**C**	**D**	**E**
$\boldsymbol{\theta}_i$ [rad]	$[0\ 0\ 0\ 0\ -0.5\pi\ 0]$	$[0\ 0\ 0\ 0\ -0.5\pi\ 0]$	$[0 - 0.4\pi\ 0\ 0 - 0.15\pi\ 0]$	$[0 - 0.35\pi\ 0\ 0 - 0.15\pi\ 0]$	$[-0.3\pi\ \ -0.2\pi\ 0\ 0 - 0.5\pi\ 0]$
$\mathbb{W}$	$(0,\ 0, ..., 0)$	$(0.2,\ 1, ..., 0)$	$(0,\ 1, ..., 0)$	$(0.2,\ 1..., 0)$	$(0.2,\ 1..., 0)$

Human Body Parameters: HBPs, Exoskeleton Parameters: EP, Inequality Constraints: ICs, Cartesian position vector: $\boldsymbol{p}$, Joint angles vector: $\boldsymbol{\theta}$.

that are the wrist and hand frame are not considered as a joint. Instead, those two frames are defined as a fixed point for the forward kinematic calculations of hand with respect to Σ_G. The position vectors between Σ_S, Σ_W, Σ_E, and Σ_H are stated as follows:

$$\boldsymbol{O_1O_2} = (l_{12_1})\boldsymbol{x} - (l_{12_2})\boldsymbol{y} - (l_{12_3})\boldsymbol{z}, \tag{1}$$

$$\boldsymbol{O_2O_3} = -(l_{23_1})\boldsymbol{x} - (l_{23_2})\boldsymbol{y} - (l_{23_3})\boldsymbol{z}, \tag{2}$$

$$\boldsymbol{O_{34}} = -(l_{34_3})\boldsymbol{z}, \tag{3}$$

where l_{ij_h} denotes the distance between i^{th} and j^{th} points along h^{th} principal axis. For instance, $\boldsymbol{O_1O_2}$, $\boldsymbol{O_2O_3}$, $\boldsymbol{O_3O_4}$ are the position vectors, and their numerical values are illustrated in Table I. First one represents the location of elbow joint relative to shoulder. Second vector shows the location of elbow joint with respect to wrist frame, and the last one defines the position of wrist with respect to hand frame.

In the next step, the dynamic model of the arm in joint space can be written based on Lagrangian formulation. The generalized coordinates are defined as $\boldsymbol{\theta} \in \mathbb{R}^n$, for n-DoFs arm. Thus:

$$\boldsymbol{B}(\boldsymbol{\theta})\ddot{\boldsymbol{\theta}} + \boldsymbol{C}(\boldsymbol{\theta}, \dot{\boldsymbol{\theta}})\dot{\boldsymbol{\theta}} + \boldsymbol{g}(\boldsymbol{\theta}) = \boldsymbol{\tau} - \overbrace{\boldsymbol{J}(\boldsymbol{\theta})^T \boldsymbol{F}_{ext}}^{\boldsymbol{\tau}_{ext}}, \tag{4}$$

where $\boldsymbol{B}(\boldsymbol{\theta})$, and $\boldsymbol{C}(\boldsymbol{\theta}, \dot{\boldsymbol{\theta}})$ are $n \times n$ inertia and coriolis/centrifugal matrix, respectively. In addition, $\boldsymbol{g}(\boldsymbol{\theta})$ is the vector of gravity joints torques, and $\boldsymbol{\tau}$ is the vector of joint torques human applies to achieve the motion. $\boldsymbol{F}_{ext} \in \mathbb{R}^k$ is the external forces/moments vector, and its effect in joint space is computed via $\boldsymbol{\tau}_{ext}$. Finally, the Jacobian matrix is defined as $\boldsymbol{J}(\boldsymbol{\theta}) \in \mathbb{R}^{k \times n}$, where $k = 6$ at the human hand in Cartesian space, and $n = 6$ in joint space.

As previously mentioned, since the control framework is designed for quasi-static movements (i.e., slow motions), a simplified approach for calculating overloading joint torques (i.e., torque values imposed on human arm joints due to external interactions) is applied as follows

$$\boldsymbol{\tau} = \boldsymbol{J}(\boldsymbol{\theta})^T \boldsymbol{F}_{ext}, \tag{5}$$

where the components of $\boldsymbol{F}_{ext}$ can be measured through the cobot's Cartesian forces, with an additional force in the z direction accounting for any object weight held by the user. Here, each component of the forward kinematics function for translational, and rotational movement is specified by the x, y, z, and φ, ϑ, ψ (RPY), respectively. As presented in Fig. 2(b), the only external force occurs along $-z$ axis due to the tool (W_P) user holds. The forearm weight (i.e., internal loading) represented with W_a is not taken into account here since it is fully compensated with the help of an exoskeleton support that will be mentioned later.

B. Online Optimization

In this chapter, online optimization formulation is studied to obtain an arm configuration such that the overloading joint torques are minimized. In the optimization problem, motion range of the joints, and cartesian movement limits are determined as the inequality constraints. Next, the cost function is built, and Frobenius norm $||.||$ is utilized to find its local minima. Therefore:

$$\theta f_0(\boldsymbol{\theta}) = ||\boldsymbol{\tau}^T \mathbb{W} \boldsymbol{\tau}||$$

$$\text{subject to} \begin{cases} f_1(\boldsymbol{\theta}) = \boldsymbol{\theta}_L - \boldsymbol{\theta} \leq 0, & f_3(\boldsymbol{\theta}) = \boldsymbol{p}_L - \boldsymbol{r} \leq 0 \\ f_2(\boldsymbol{\theta}) = \boldsymbol{\theta} - \boldsymbol{\theta}_U \leq 0, & f_4(\boldsymbol{\theta}) = \boldsymbol{p} - \boldsymbol{p}_U \leq 0 \end{cases} \tag{6}$$

where $\boldsymbol{p} \in \mathbb{R}^{k\times 1}$ is the vector of positions in task space, and defined within the robot workspace. $\mathbb{W} \in \mathbb{R}^{k\times n}$ is a symmetric positive definite weight matrix, and each diagonal member of it (7) corresponds to the joint numbers. Moreover, $\boldsymbol{\theta}_L, \boldsymbol{p}_L$, and $\boldsymbol{\theta}_U, \boldsymbol{p}_U$ signify the lower and upper boundary of the inequality constraints, respectively.

$$\mathbb{W} = \text{diag}(W_1, W_2, \ldots, W_n). \tag{7}$$

Augmented Lagrangian solver (AUL) of ALGLIB library is employed for the minimization of the objective function. In this method, first gradient of the functions including objective and inequality constraints should have non-zero values at the determined boundary. By assigning different weights to the shoulder and elbow joints, various arm configurations can be achieved. The choice of weights depends on which joints require minimized overloading torques. For instance, in the case of the elbow exoskeleton, the weight will remain zero until the exoskeleton reaches its full torque capacity. The range of weight is also important during the tuning process. It is stated that the relative differences among weights are more important than their independent absolute values [25]. Hence, the range is specified between 0 and 1. For instance, specifying $W_2 \approx 1$ and $W_5 \approx 0$ generates a similar arm configuration as in Fig. 2(b), that is, minimum torque at the shoulder ($\theta_2 \approx 0^\circ$), and max torque at the elbow ($\theta_5 \approx -90^\circ$). More discussion and concrete results about the effects of weight on the cost function are presented in Section III.

C. Robot Planning

Once an optimal configuration for the human arm is achieved, the robot's path planner aims to help the user reach a similar arm configuration. Simultaneously, real-time visual feedback is provided to the user via an avatar displaying both the optimized pose and the actual pose, as shown in Fig. 1. The user then adjusts their arm to align the actual pose with the optimized one, with the robot following this movement. During this process, the robot tracks the human hand, allowing the painting task to be completed with reduced effort and under the user's supervision. To enable this, a target frame Σ_T is defined with a translational offset (e) relative to the hand frame (see Fig. 2). The robot is then controlled to follow this target along a linear trajectory, calculated based on the reaching time and the positional error between the target and the robot's end-effector frame ($\delta \boldsymbol{r}$). A Cartesian impedance controller is developed for the trajectory tracking, and to achieve a compliant behaviour at the robot end-effector.

D. Exoskeleton Assistance

Even though optimization of the joint angles can reduce the overloading joint torques through the assistance of the robot, the remaining effort on the user's joints is still not trivial due to the external and internal loading's. To amplify the physical support to the worker, an elbow assistive device is attached to the user without preventing the arm movements in 3D space during the robot path planning. The actuation system of the device is developed through series elastic actuation (SEA) principle. An endless shape bungee element is elongated linearly by the ball-screw and a DC motor (ECXTQ22XL, GPX22UP) to generate the desired force in a compliant way. The support that device provides cover the entire forearm weight (W_a) and some portion of the external load (W_P) as shown in Fig. 2. The assistive torque (τ_{Exo}) about O_2 is computed as follows:

$$\tau_{Exo} = \overbrace{W_l \sin(\theta_5) l_L}^{\tau_L} + \overbrace{W_a \sin(\theta_5) l_A}^{\tau_A}, \quad F_R = \frac{\tau_{Exo}}{L\cos(\gamma)} \tag{8}$$

where $l_A = b + c$, and $l_l = b + c + d$ are the lever length for the forearm and the external load, respectively. W_l is the external load that the device can fully compensate, and it is smaller than the actual load (W_P). The force trajectory to transfer this torque to the elbow joint is represented with F_R, which includes some geometrical relations of the arm attachments, forearm weight, external load, and joint angle as the variable. Thus, the motion change on the elbow joint is captured via an encoder and F_R is updated while measuring the tendon force by means of a load cell (FUTEK-LSB201). The resultant error is fed to a PID controller as input, and the output is computed as the new bungee elongation. More details about the design and control of the mechanism can be found in [20], [26].

III. Experiments & Results

An equivalent industrial painting task (see Fig. 1) is designed to evaluate the developed control framework on 4 young healthy subjects (30 ± 5 years old), and the experiments were conducted at the Human-Robot Interfaces and Interaction (HRII) Lab, Istituto Italiano di Tecnologia (IIT), and approved by the ethics committee Azienda Sanitaria Locale (ASL) Genovese N.3 (Protocol IIT HRII SOPHIA 554/2020).

The flowchart of the experiments is presented in Fig. 3. First, the XSens MVN suit is worn by the subjects for full-body motion capture as in Fig. 1. However, since our interest is to monitor only upper-body motions, 11 miniature inertial measurement units (IMU) are used in the experiments. The frame locations of human joints w.r.t Σ_0 are acquired in ROS (Robot Operating System) through the software framework [27]. Afterward, a closed loop inverse kinematic (CLIK) algorithm [28] is implemented to estimate the joint angles in their local frame. Next, those joint angles and human body parameters (HBPs in Table I) are fed to our URDF model, where the global frame is attached in the shoulder (see Fig. 2(a)), to estimate the joint torques through (5). After that, those torques are employed in the cost function together with the weight matrix to minimize the overloading joint torques. As the exoskeleton compensates the torque load for elbow flexion/extension movement (θ_5), W_5 element of the weight matrix is set always 0. In addition, minimizing θ_3, θ_4, and θ_6 is not our objective, as it is not relevant to our specific use cases within the context of a European project. Additionally, [3] demonstrates that the primary loaded joints in a painting task are θ_1, θ_2, and θ_5. Thus W_3, W_4, and W_6 are assigned as 0 as in Table I. However, W_1, and W_2 are varied in each test. As mentioned in Section II-B, to achieve a different priority in the optimization, it is important to evaluate the ratio between the elements of $\mathbb{W}$ rather than their absolute values. Therefore, W_1, and W_2 are determined as 0.2, and 1 (or vice versa) among the tests to monitor how θ_1, and θ_2 are changed as a result of the optimization process. Moreover, the inequality constraints are defined for the position limits in task space ($\boldsymbol{r_L}, \boldsymbol{r_U}$) and the joint angle limits ($\boldsymbol{\theta_L}, \boldsymbol{\theta_U}$) based on the painting task requirements. Also, the optimization is performed at different initial arm configurations represented in $\boldsymbol{\theta_i}$. Next, the Franka Emika Panda robot is operated through a custom ROS controller, and a calibration session is performed. To map the hand movements (defined in Σ_0) in Σ_B, Σ_{EE} and Σ_H are

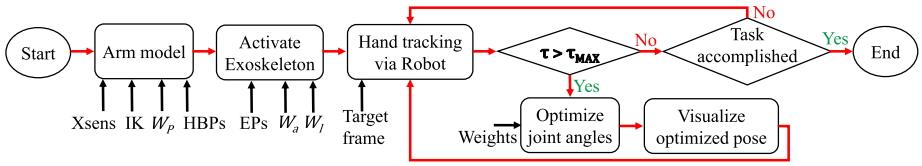

Fig. 3. Proposed control strategy to alleviate the overloading joint torques by means of the robot and the elbow exoskeleton. IK and HBPs represent the inverse kinematics, and human body parameters, respectively. Black arrows are the inputs whereas red arrows show the flow of the control algorithm.

closely coincided at the calibration pose in sagittal plane which corresponds to keeping their fist below the Σ_{EE} around $\theta_2 \approx 0°$ and $\theta_5 \approx -90°$ (all the other joints are $\approx 0°$). The measured error between Σ_{EE} and Σ_H is adjusted to be almost zero by changing the Σ_B in RVIZ (ROS graphical interface), and participants are asked to stay at the same location throughout the experiment. After this calibration, the target frame (Σ_T) is created $e = 20$ mm ahead of the Σ_H, and tracked by the robot in translational movements. The assigned stiffness gains for the cartesian impedance controller are $K_x = K_y = K_z = 600$ N/m, $K_{roll} = K_{pitch} = K_{yaw} = 30$ Nm/rad, and damping gains are set proportionally.

Regarding the assistive device, first, the parameters including a, b, c, and d (see Table I) are set for all subjects, and a PID based force control ($K_{P_f} = 0.1, K_{I_f} = 6, K_{D_f} = 0.002$) is implemented in MATLAB/Simulink Real-Time interface to track the force reference generated based on (8). Also, a data acquisition card and a motor driver are communicated via an EtherCAT at 1 kHz. In the experiments, Wagner56652/2017 paint sprayers ($W_P = 2$ and 4kg) are held by the subjects as the external load. In (8), the forearm weight is set as 20 N for all subjects considering [21] whereas the external load (W_l) is assigned to be 10 N (max permissible external load value). During the experiments, to monitor the effort reduction on shoulder (flexion/extension and abduction/adduction) and elbow joint movements (flexion/extension), the muscular activities of anterior deltoid (AD), middle deltoid (MD), posterior deltoid (PD), and biceps brachii (BB) are recorded via the wireless sEMG device of Delsys Trigno platform by Delsys Inc (Natick, MA, United States). The EMG raw data is obtained at 2 kHz, then it is post-processed in MATLABapplying a second order high-pass filter with 0.1 Hz. Finally, full-wave rectification is carried out, and 2.5 Hz second-order low pass filter is employed on the data.

A. Experimental Protocol

Each subject participated in 8 tests, with the optimization parameters presented in Table I. Experiments A and B were conducted with the exoskeleton, while C, D, and E were carried out both with (W/) and without (W/O) the exoskeleton. The test order was randomized as in [29]. Additionally, while a weight of $W_P = 4$ kg was used in experiment B, a weight of $W_P = 2$ kg served as the external load for all other tests.

In each experiment, subjects first stayed at the calibration location with the cobot. They were then instructed to position their arm to the initial pose (within a tolerance of $\pm 0.03\pi$) shown as $\boldsymbol{\theta}_i$ in Table I. Afterward, the cobot was activated and moved to Σ_T to track the user's hand until the actual arm pose aligned with the optimized pose (avatar). For tests conducted with assistance, the steps described above were completed with exoskeleton support. Additionally, a tolerance was introduced

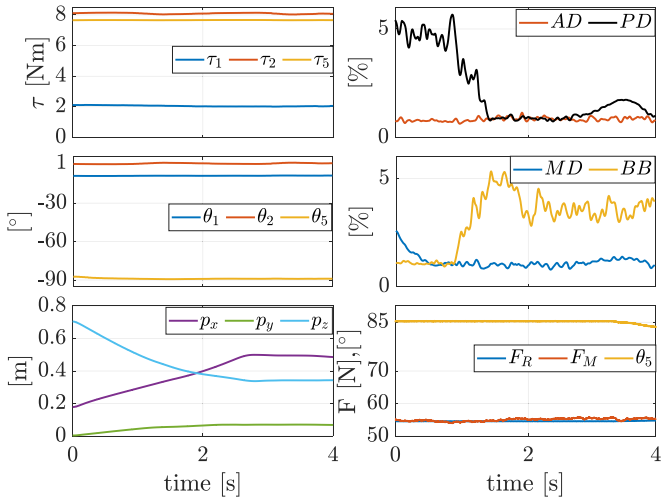

Fig. 4. Experiment-A results of S_1 where 2kg payload is held by assigning null value in $\mathbb{W}$ to record $\boldsymbol{\tau_{Max}}$ at a predetermined pose. F_R, and F_M are the desired and measured force of the exoskeleton, respectively.

for the error between the optimized angle of the target joint (i.e., θ_1, θ_2, θ_5) and the actual joint angle, set to $\theta_E = 10° \pm 5°$, to account for possible inconsistencies in movement coordination among subjects. In experiment-A, the $\mathbb{W}$ is defined as null, and thus no solution is expected from the optimization algorithm. The goal is to acquire the maximum allowable joint torques ($\boldsymbol{\tau_{Max}}$) whose surpassing leads to trigger the optimization for the following tests. In experiment-B, the external load is doubled at the same $\boldsymbol{\theta_i}$ as the experiment-A, and hence the $\boldsymbol{\tau_{Max}}$ is exceeded. Here, the optimization is carried out by determining W_2 greater than W_1 since the aim is to distribute the torque load among θ_2, and θ_5 while alleviating τ_1. In experiment-C, $\boldsymbol{\theta}_i$, and W_P are changed while assigning only a nonzero W_2 to monitor if the optimization can reduce the effort about only θ_2. When it comes to experiment-D, in addition to W_2, W_1 is assigned to observe the torque reduction about both θ_1, and θ_2 with almost similar $\boldsymbol{\theta}_i$ as previous test. Finally, experiment-E is carried out by making use of the same weight matrix as experiment-D, yet the $\boldsymbol{\theta}_i$ is modified to amplify the initial torque of the shoulder about θ_1, and θ_2.

B. Experimental Results

The average value of all subjects' data with standard deviation (std) for experiments B, C, D, and E are reported in Table II. Since experiment-A is carried out only to determine the $\boldsymbol{\tau_{Max}}$ values without assigning a nonzero weight in the optimization, its results are excluded here. To start with, θ_{1E}, θ_{2E}, and θ_{5E} represent the error between the optimized and the actual pose of the corresponding joints, and they are reported to monitor how

TABLE II
EXPERIMENT RESULTS. THE VALUE IS REPORTED AS: MEAN (STANDARD DEVIATION)

	B		C		D		E	
	W/	W/O	W/	W/O	W/	W/O	W/	W/O
θ_{1E}	8.6 (4.2)	-	2.6 (2.5)	1.7 (0.8)	6.5 (2)	4.3 (2.6)	7 (2.4)	5.8 (6.1)
θ_{2E}	4.8 (2.7)	-	6.1 (6.2)	8.9 (4.1)	6.2 (3.9)	9.8 (5.1)	11.9 (1.1)	9.1 (5.3)
θ_{5E}	8.3 (7.8)	-	7.2 (6.5)	6.2 (2.6)	9.1 (5.4)	3.2 (2.7)	7.7 (3.1)	5.3 (1.8)
F_E [N]	1.9 (0.9)	-	1.9 (0.7)	-	1.8 (0.4)	-	2.6 (0.7)	-
P_E [mm]	10.3 (2.3)	-	9.3 (1.1)	9.9 (2.3)	10.4 (4.9)	10.2 (3.2)	8.8 (0.9)	8.1 (1.6)
τ_1 [%]	102.1 (68.8)	-	99.4 (1.1)†	98.6 (2.8)†	80.9 (22.2)†	93.6 (12.4)†	−52.7 (30.3)	−56.7 (15.2)
τ_2 [%]	−44.6 (17.2)	-	−51.3 (4.1)	−51.8 (4.2)	−46.2 (4.8)	−48.5 (5.5)	−31.4 (1.7)	−31.2 (3.4)
τ_5 [%]	−24.8 (10.4)	-	6 (1.4)	21.1 (16.4)	15.8 (13.6)	22.8 (14.8)	18.2 (21.4)	17.9 (8.1)
BB	5.86 (4.7)	-	6.52 (4.14)	10.16 (5.89)	6.81 (3.89)	10.24 (6.31)	4.14 (2.12)	7.96 (5.04)
AD	2.9 (2.8)	-	21.3 (8.6)	20.5 (7.6)	21.8 (9.6)	24.2 (12.6)	14.7 (8.6)	7.5 (0.9)
MD	3.3 (1.8)	-	20.2 (9.73)	17.58 (5.73)	14.23 (10)	11.5 (6.12)	12.6 (6.6)	15.6 (8.01)
PD	6.45 (4.54)	-	6.1 (2.98)	5.35 (1.65)	4.4 (2.75)	5.12 (3.52)	4 (2.3)	3.9 (1.47)

θ_{1E}, θ_{2E}, and θ_{5E} are the error between optimized and the actual pose. F_E is the force tracking error of the exoskeleton while P_E is the RMS value of the cartesian error in x, y, z axis of the robot. τ_i [%] for $i = 1, 2, 5$ represents the change of the torque at the defined joint.

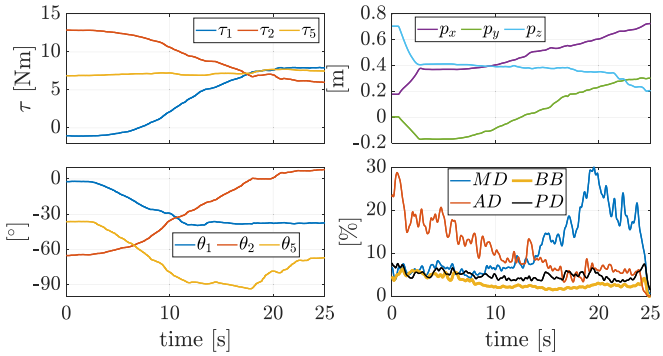

Fig. 5. Experiment-C results of S_3 in which $W_P = 2$ kg payload is held without wearing the assistive device. F_R, and F_M are the desired and measured force of the exoskeleton, respectively. τ is the joint torque.

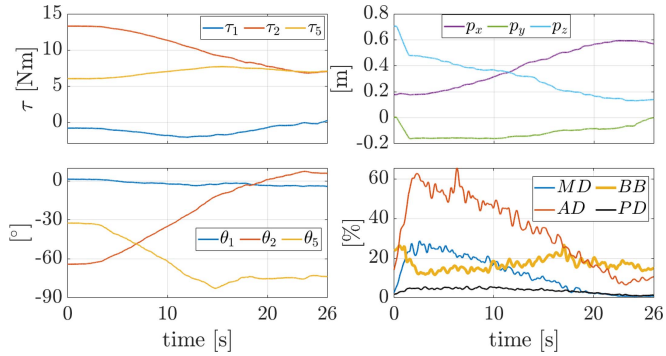

Fig. 7. Experiment-D results of S_2 in which $W_P = 2$ kg payload is held without wearing the assistive device. F_R, and F_M are the desired and measured force of the exoskeleton, respectively. τ is the joint torque.

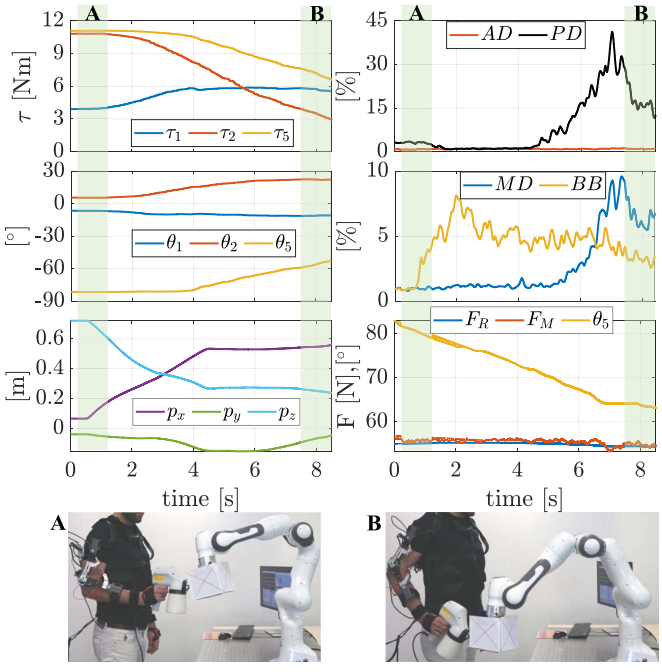

Fig. 6. Experiment-B results of S_1 where 4kg payload is held by assigning nonzero W_1, and W_2. F_R, and F_M are the desired and measured force of the exoskeleton, respectively. τ is the joint torque.

close the subjects' arm pose to that of the provided optimized one. They are calculated by taking the average value of the last 3 seconds of the corresponding joint angle (i.e., after optimization) for each test, and subtracted from that of the optimized angle. Next, F_E, and P_E are the RMS value of the force error of the exoskeleton, and the Cartesian error in x, y, z axes of the robot, respectively. The latter is computed taking the RMS value of the error along each axis during the test, and then the RMS value of the error for all axes is computed. Moreover, the rate of change of torques in percentage for θ_1, θ_2, θ_5 are reported by taking the average of the first and last 3 seconds of the data as illustrated in Fig. 9 with state-A and B. Then, the torque difference between the two states is divided to the initial torque, and multiplied by 100 to compute the reduction or increment percentage with respect to the initial state. However, there is an exception that is employed for 4 tests pointed with † on the Table II. To clarify, since the final τ_1 value of those tests are drastically higher than that of the initial one (i.e., the initial condition of θ_1 is 0 for these tests), their rate of change is computed considering the final state to make the data interpretation easier. Furthermore, to monitor the effort change among the tests, RMS values of EMG channels including AD, MD, PD, and BB are computed for each test.

To begin with, according to the results of experiment-A in Fig. 4, the $\boldsymbol{\tau_{Max}}$ are recorded as $\tau_1 = 2.02$ Nm, $\tau_2 = 8.13$ Nm, $\tau_5 = 7.66$ Nm. No movement is performed by S_1 since a null $\mathbb{W}$ is set. Considering the exoskeleton support ($F_R \approx 55$

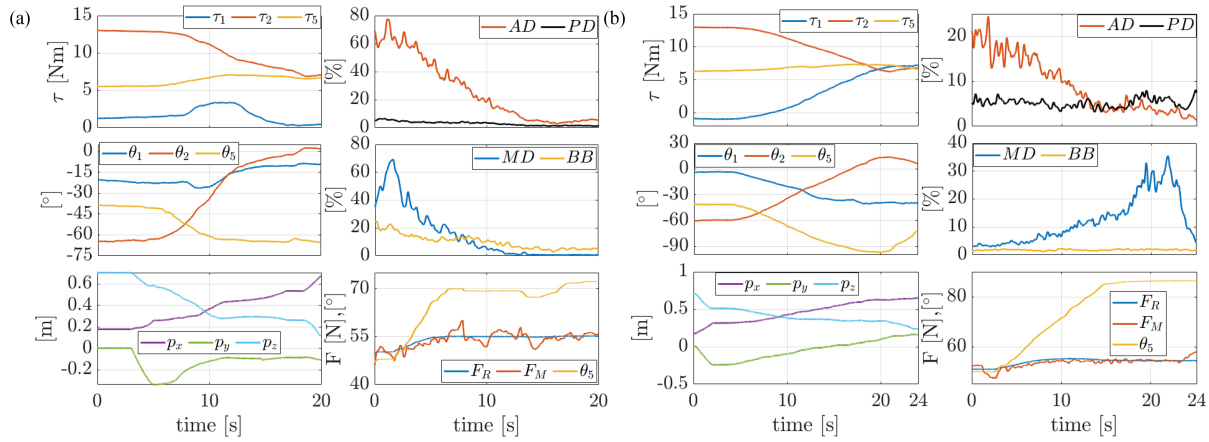

Fig. 8. (a) The experiment-D results of S_2, and (b) the experiment-C results of S_3. Both tests are conducted under exoskeleton support by holding $W_P = 2$ kg. F_R, and F_M are the desired and measured force of the exoskeleton, respectively. τ is the joint torque.

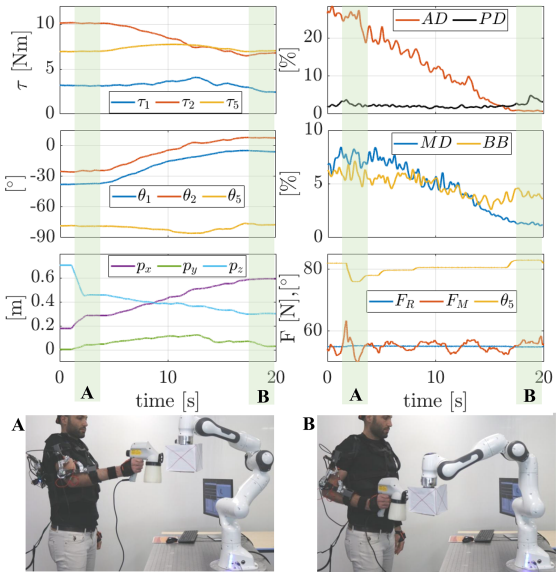

Fig. 9. Experiment-E results of S_1 in which 2kg payload is held by assigning nonzero W_1, and W_2. F_R, and F_M are the desired and measured force of the exoskeleton, respectively. τ is the joint torque.

N generates ≈ 6 Nm assistive torque at elbow joint based on (8)), it is clear that the resultant τ_5 is quite low.

Next, in experiment-B, since $\boldsymbol{\tau_{Max}}$ is surpassed due to the change of payload (see Fig. 6 state A), the optimization provides a new arm configuration by extending the shoulder and elbow to distribute the torque load among those joints. Note that at state-B, joint torques, and EMG signals bear close and even smaller values than that of experiment-A within the Cartesian limits ($\boldsymbol{p}$) thanks to the control framework. The muscular activation also points out the aforementioned shoulder extension movement in Table II, that is, the AD contracts 53.7% less than that of PD. Finally, the small increment of τ_1 in Fig. 6 is due to the structure of the exoskeleton, which partially restricts the user from moving the arm to the fully adducted shoulder. This situation can be seen in its std values in Table II as well, demonstrating a large fluctuation in the overall data.

Regarding the experiment-C results in Figs. 8(b) and 5, even though there is a sharp torque reduction about θ_2, the optimized pose amplifies the torque about θ_1 due to the assigned zero W_1. Therefore, MD is 82.4% higher than that of experiment-B in Table II. On the other hand, even though the values of τ_5 are similar in both figures, the BB contraction is three times smaller in W/ assistance than W/O, showing the impact of the exoskeleton. Also, the small differences in robot Cartesian movements between both figures verifies the implementation of the same initial conditions (i.e., $\boldsymbol{\theta_i}$, and $\mathbb{W}$).

When it comes to experiment-D results, τ_1 decreases significantly (i.e., 5 times smaller than experiment-C) because of nonzero W_1 as in both Figs. 8(a) and 7. Hence, MD is 31.8% less than that of experiment-C according to Table II, validating the abovementioned torque alleviation.

Afterward, according to experiment-E results in Fig. 9, τ_1 at state-A is greater than all the other experiments due to the initial nonzero θ_1 values. Eventually, at state-B, the efforts in the shoulder and elbow are mitigated thanks to the developed control framework. Furthermore, the average τ_1 reduction is notable, reaching 54.7% ($\pm$10.6) in Table II.

Finally, some general conclusions are drawn to demonstrate the effectiveness of the proposed control framework. For instance, in Table II, the mean value ($\pm$ std) of θ_{1E}, θ_{2E}, θ_{5E}, F_E, and P_E of all experiments of participants are 5.22° ($\pm$3.78), 8.13° ($\pm$4.51), 6.72° ($\pm$4.62), 2.08N ($\pm$0.37 N), and 9.6mm ($\pm$0.87 mm), respectively. It is clear that the participants are guided via the avatar in the predetermined θ_E tolerance for three angles. Moreover, the small error of F_E shows that the exoskeleton assistance is provided successfully to the subjects, and this error can be improved through more precise gain tuning. Furthermore, the marginal error of P_E verifies the hand tracking performance of the robot. In addition, since a nonzero W_2 is defined for all tests, the average τ_2 reduction and its standart deviation are substantial, bearing 43.6% ($\pm$5.8). Another point is related to muscle activation. To clarify, as the initial θ_2 values of experiment-C, and D are slightly different, AD contraction of them are close to each other (see Table II). Yet, the initial θ_2 of experiment-E is smaller than those experiments, and thus its AD contraction is 46.8% less than that of those experiments. Finally, a major effort reduction is observed in BB muscle thanks to the elbow exoskeleton between W/ and W/O assistance, pointing 35.8%, 33.5%, and 47.9% with respect to W/O for test-C, D and E, respectively. Furthermore, the rate of change of τ_5 increases in most of the tests due to assigned zero W_5 except test-B. In this test, even though a nonzero W_1, and W_2 are set, since θ_1 is already 0in the beginning, the main priority is given to the

minimization of θ_2. In this case, the optimization provides an arm configuration such that the center of mass of the upper and lower arm are almost aligned along the z axis of the Σ_G (see the arm configuration at state-B in Fig. 6(b)). To achieve this, the θ_5 is reduced by the optimization, and hence τ_5 is mitigated in test-B.

IV. Conclusion & Future Study

In this letter, we designed a control framework to alleviate the overloading joint torques in manual operations with the help of a cobot and a lightweight elbow exoskeleton. Through an anticipatory optimisation of the human arm configuration and cobot path planning, our framework enabled the users to align the external loads with the exoskeleton-supported joints to the maximum extent possible. Results show that the mean value of θ_{1E}, θ_{2E}, and θ_{5E} of all subjects of all experiments is $6.69 \pm 4.43°$, concluding that the participants followed the visual feedback with minimal error. As a result of this small error, the mean value of the optimized joint torques of all subjects for τ_1, τ_2, and τ_5 are $3.63{\pm}0.85$ Nm, $6.83{\pm}0.47$ Nm, and $7.2{\pm}0.28$ Nm, respectively. It is clear that τ_1 is slightly above the predetermined max threshold, yet τ_2, and τ_5 are significantly below than that of the τ_{Max} values. Given the support of the exoskeleton, which is ≈ 6 Nm for all subjects, the measured τ_5 on participants is quite less, settling around 1 Nm. The marginal increment of τ_1 is due to the assigned $W_1 = 0$ in test-C, which increases the mean value. However, we assigned it intentionally to demonstrate the performance of the optimization under different $\mathbb{W}$.

Regarding the limitations of our framework, it cannot be applied in a task where a human bends or takes a step to move to another position due to the predetermined calibration location. Thus, this calibration process should be improved so that the method can be implemented in a variety of applications in real workstations. Also, we developed the human model for quasi-static movements, neglecting the dynamic effects. Hence, future studies will overcome those challenges by extending the framework to multi DoFs (full-body model) with several lightweight exoskeletons while varying $\mathbb{W}$ adaptively in a dynamic use case, and performing statistical analysis (e.g., NASA) on a higher number of subjects.

References

[1] M. Napolitano, "2012 warehouse/DC operations survey: Mixed signals," *Logistics Manage. (Highlands Ranch, Colo.: 2002)*, vol. 51, no. 11, pp. 54–63, 2012.

[2] B. Vanderborght, *Unlocking the Potential of Industrial Human–Robot Collaboration: A Vision on Industrial Collaborative Robots for Economy and Society*. European Commission: Pub. Office Eur. Union, 2020.

[3] P. M. Rosati, J. N. Chopp, and C. R. Dickerson, "Investigating shoulder muscle loading and exerted forces during wall painting tasks: Influence of gender, work height and paint tool design," *Appl. Ergonom.*, vol. 45, no. 4, pp. 1133–1139, 2014.

[4] K. L. Hunting, J. A. Murawski, and L. S. Welch, "Occupational injuries among construction workers treated at the George Washington University emergency department, 1990-97," in *Proc. Center Protect Workers' Rights*, 2004, pp. 1–23.

[5] C. H. Glock, E. H. Grosse, W. P. Neumann, and A. Feldman, "Assistive devices for manual materials handling in warehouses: A systematic literature review," *Int. J. Prod. Res.*, vol. 59, no. 11, pp. 3446–3469, 2021.

[6] D. Ranney, R. Wells, and A. Moore, "Upper limb musculoskeletal disorders in highly repetitive industries: Precise anatomical physical findings," *Ergonomics*, vol. 38, no. 7, pp. 1408–1423, 1995.

[7] S. Haddadin and E. Croft, "Physical human–robot interaction," in *Springer Handbook of Robotics*, Cham, Switzerland: Springer Cham, 2016, pp. 1835–1874.

[8] S. Chen et al., "Wearable knee assistive devices for kneeling tasks in construction," *IEEE/ASME Trans. Mechatron.*, vol. 26, no. 4, pp. 1989–1996, Aug. 2021.

[9] A. Madani, P. P. Niaz, B. Guler, Y. Aydin, and C. Basdogan, "Robot-assisted drilling on curved surfaces with haptic guidance under adaptive admittance control," in *Proc. 2022 IEEE/RSJ Int. Conf. Intell. Robots Syst.*, 2022, pp. 3723–3730.

[10] R. Zhang, Q. Lv, J. Li, J. Bao, T. Liu, and S. Liu, "A reinforcement learning method for human-robot collaboration in assembly tasks," *Robot. Comput.- Integr. Manuf.*, vol. 73, 2022, Art. no. 102227. [Online]. Available: https://www.sciencedirect.com/science/article/pii/S0736584521001095

[11] D. Colley, C. D. Bowersock, and Z. F. Lerner, "A lightweight powered elbow exoskeleton for manual handling tasks," *IEEE Trans. Med. Robot. Bionics*, vol. 6, no. 4, pp. 1627–1636, Nov. 2024.

[12] C. O'Neill et al., "Inflatable soft wearable robot for reducing therapist fatigue during upper extremity rehabilitation in severe stroke," *IEEE Robot. Automat. Lett.*, vol. 5, no. 3, pp. 3899–3906, Jul. 2020.

[13] R. Kumar, S. Lal, S. Kumar, and P. Chand, "Object detection and recognition for a pick and place robot," in *Proc. Asia-Pacific World Congr. Comput. Sci. Eng.*, 2014, pp. 1–7.

[14] L. Peternel, C. Fang, N. Tsagarakis, and A. Ajoudani, "A selective muscle fatigue management approach to ergonomic human-robot co-manipulation," *Robot. Comput.- Integr. Manuf.*, vol. 58, pp. 69–79, 2019.

[15] L. v. d. Spaa, M. Gienger, T. Bates, and J. Kober, "Predicting and optimizing ergonomics in physical human-robot cooperation tasks," in *Proc. 2020 IEEE Int. Conf. Robot. Automat.*, 2020, pp. 1799–1805.

[16] A. M. Zanchettin, E. Lotano, and P. Rocco, "Collaborative robot assistant for the ergonomic manipulation of cumbersome objects," in *Proc. 2019 IEEE/RSJ Int. Conf. Intell. Robots Syst.*, 2019, pp. 6729–6734.

[17] W. Kim, J. Lee, L. Peternel, N. Tsagarakis, and A. Ajoudani, "Anticipatory robot assistance for the prevention of human static joint overloading in human–robot collaboration," *IEEE Robot. Automat. Lett.*, vol. 3, no. 1, pp. 68–75, Jan. 2018.

[18] W. Kim, L. Peternel, M. Lorenzini, J. Babič, and A. Ajoudani, "A human-robot collaboration framework for improving ergonomics during dexterous operation of power tools," *Robot. Comput.- Integr. Manuf.*, vol. 68, 2021, Art. no. 102084.

[19] W. Kim et al., "Adaptable workstations for human-robot collaboration: A reconfigurable framework for improving worker ergonomics and productivity," *IEEE Robot. Automat. Mag.*, vol. 26, no. 3, pp. 14–26, Sep. 2019.

[20] E. Mobedi, W. Kim, M. Leonori, N. G. Tsagarakis, and A. Ajoudani, "Design and control of an assistive device for elbow effort-compensation," *IEEE/ASME Trans. Mechatron.*, vol. 28, no. 6, pp. 3446–3457, Dec. 2023.

[21] L. Cappello, A. Pirrera, P. Weaver, and L. Masia, "A series elastic composite actuator for soft arm exosuits," in *Proc. 2015 IEEE Int. Conf. Rehabil. Robot.*. IEEE, 2015, pp. 61–66.

[22] W. T. Dempster and G. R. Gaughran, "Properties of body segments based on size and weight," *Amer. J. Anatomy*, vol. 120, no. 1, pp. 33–54, 1967.

[23] MVN, "Xsens MVN biomechanical model description," 2023. Accessed: Feb. 15, 2025. [Online]. Available: https://base.movella.com/s/article/MVN-Biomechanical-Model?language=en_US#Reference

[24] G. Wu et al., "ISB recommendation on definitions of joint coordinate systems of various joints for the reporting of human joint motion—Part II: Shoulder, elbow, wrist and hand," *J. Biomech.*, vol. 38, no. 5, pp. 981–992, 2005. [Online]. Available: https://www.sciencedirect.com/science/article/pii/S002192900400301X

[25] R. T. Marler and J. S. Arora, "The weighted sum method for multi-objective optimization: New insights," *Struct. Multidisciplinary Optim.*, vol. 41, pp. 853–862, 2010.

[26] E. Mobedi, S. Hjorth, W. Kim, E. D. Momi, N. G. Tsagarakis, and A. Ajoudani, "A power-aware control strategy for an elbow effort-compensation device," *IEEE Robot. Automat. Lett.*, vol. 8, no. 7, pp. 4330–4337, Jul. 2023.

[27] M. Leonori, M. Lorenzini, L. Fortini, J. M. Gandarias, and A. Ajoudani, "The bridge between Xsens motion-capture and robot operating system (ROS): Enabling robots with online 3D human motion tracking," 2023, *arXiv:2306.17738*.

[28] J. Carpentier et al., "The Pinocchio C++ library : A fast and flexible implementation of rigid body dynamics algorithms and their analytical derivatives," in *Proc. 2019 IEEE/SICE Int. Symp. System Integration*, 2019, pp. 614–619.

[29] M. Schalk, I. Schalk, T. Bauernhansl, J. Siegert, A. Esin, and U. Schneider, "Influence of exoskeleton use on welding quality during a simulated welding task," *Wearable Technol.*, vol. 3, 2022, Art. no. e17.